Joule

CellPress

Article

Hybrid Aqueous/Non-aqueous Electrolyte for Safe and High-Energy Li-Ion Batteries

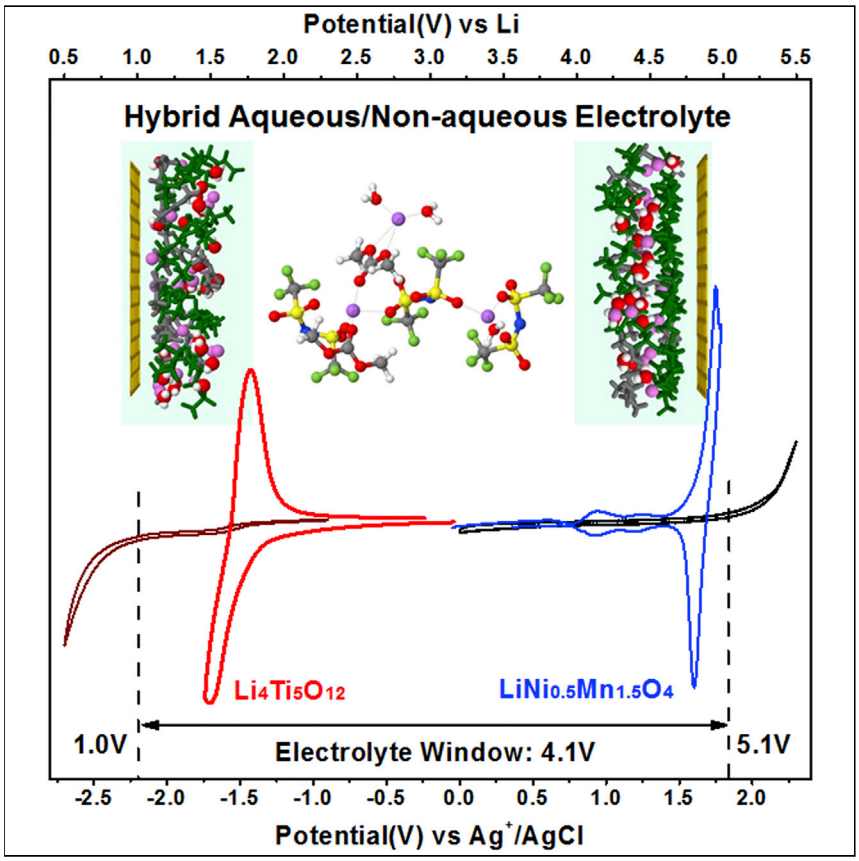

Hybrid aqueous/non-aqueous electrolyte (HANE) inherits the merits from both aqueous (non-flammability) and non-aqueous (high electrochemical stability) systems. Its unique assembly at the inner-Helmholtz interface leads to an interphasial chemistry that supports a 3.2 V $Li_4Ti_5O_{12}/LiNi_{0.5}Mn_{1.5}O_4$ full aqueous Li-ion battery with performances comparable with state-of-the-art Li-ion batteries.

Fei Wang, Oleg Borodin, Michael S. Ding, ..., Steve Greenbaum, Kang Xu, Chunsheng Wang

conrad.k.xu.civ@mail.mil (K.X.)
cswang@umd.edu (C.W.)

HIGHLIGHTS

A new hybrid aqueous/non-aqueous electrolyte (HANE) is demonstrated

HANE inherits merits from electrolytes of both aqueous and non-aqueous natures

Investigated the evolution of inner-Helmholtz interface under different potentials

The interphase chemistry allows a 3.2 V $Li_4Ti_5O_{12}/LiNi_{0.5}Mn_{1.5}O_4$ full cell

Wang et al., Joule 2, 1–11
May 16, 2018 Published by Elsevier Inc.
https://doi.org/10.1016/j.joule.2018.02.011

Please cite this article in press as: Wang et al., Hybrid Aqueous/Non-aqueous Electrolyte for Safe and High-Energy Li-Ion Batteries, Joule (2018), https://doi.org/10.1016/j.joule.2018.02.011

Joule

CellPress

Article

Hybrid Aqueous/Non-aqueous Electrolyte for Safe and High-Energy Li-Ion Batteries

Fei Wang,[1,2] Oleg Borodin,[2] Michael S. Ding,[2] Mallory Gobet,[3] Jenel Vatamanu,[2] Xiulin Fan,[1] Tao Gao,[1] Nico Edison,[1] Yujia Liang,[1] Wei Sun,[1] Steve Greenbaum,[3] Kang Xu,[2,4,*] and Chunsheng Wang[1,*]

SUMMARY

Recent breakthroughs in aqueous electrolytes made highly safe 3.0 V class aqueous Li-ion batteries possible. However, the formed solid-electrolyte interphase therein still cannot effectively support the desired energy-dense anode and cathode materials. In this work, we report a new class of electrolytes, by hybridizing aqueous with non-aqueous solvents, that inherits the non-flammability and non-toxicity characteristics from aqueous and better electrochemical stability from non-aqueous systems. The secondary interphasial ingredient (alkylcarbonate) introduced by non-aqueous component helps to expand the electrochemical window of the hybridized electrolyte to 4.1 V, which supports the operation of a 3.2 V aqueous Li-ion battery based on $Li_4Ti_5O_{12}$ and $LiNi_{0.5}Mn_{1.5}O_4$ to deliver a high energy density of 165 Wh/kg for >1,000 cycles. The understanding of how a better interphase could be tailored by regulating the inner-Helmholtz interfacial structures of the hybridized electrolyte provides important guidelines for designing future electrolytes and interphases for new battery chemistries.

INTRODUCTION

The impact of lithium-ion batteries (LIBs) can be felt ubiquitously in our life, from portable electronics and electric vehicles to grid-storage applications,[1,2] while their limited energy densities often inconvenience our daily schedule, accessibility, and mobility. The push for new battery chemistries with higher energy density and increased safety has become ever stronger, especially in the presence of the rare but high-profile safety incidents highlighted by the news media.[3–6] LIBs based on aqueous electrolytes attract intense attention due to their intrinsic non-flammable nature, high tolerance against abuse and environmental moisture, high flexibility in both form-factor and manufacturing environment, as well as little reliance on battery management systems at module or pack levels.[7–9] However, the electrochemical instability of water, as characterized by its narrow voltage window of 1.23 V, places an upper limit on their energy densities (<70 Wh/kg), excluding them completely from the category of "high-energy rechargeable batteries."[8,10–12]

This upper limit was recently breached by a new class of aqueous electrolytes.[13] Named "water-in-salt" electrolyte (WiSE) after the superconcentrated lithium salts used therein (>21 m, mol/kg, molality), such an aqueous electrolyte and its later improved derivatives can support diverse battery chemistries within its expanded voltage window of 3.0 V, with the cathodic limit located at ~1.90 V versus

Context & Scale

A new class of electrolyte is created by hybridizing aqueous and non-aqueous components. Named hybrid aqueous/non-aqueous electrolyte (HANE), it bridges the once-clear demarcation between aqueous and non-aqueous electrolytes and inherits merits from both. A Li-ion battery based on $Li_4Ti_5O_{12}$/$LiNi_{0.5}Mn_{1.5}O_4$ was demonstrated to deliver performances comparable with those of the state-of-the-art non-aqueous Li-ion batteries, as represented by the high working voltage of 3.2 V, energy density of 165 Wh/kg, and cycling stability beyond 1,000 cycles. The correlation established between solvation structure in HANE and the resultant interphase on anode surfaces provides insights for how to design a better interphase by regulating the inner-Helmholtz regions.

Please cite this article in press as: Wang et al., Hybrid Aqueous/Non-aqueous Electrolyte for Safe and High-Energy Li-Ion Batteries, Joule (2018), https://doi.org/10.1016/j.joule.2018.02.011

Li.[5,7,13–19] The significant expansion was realized via the formation of an aqueous solid-electrolyte interphase (SEI) on various anode surfaces. Unlike the interphases in state-of-the-art LIB or Li-metal batteries, which consist mainly of reduction products from the solvents and therefore are organic in nature (alkylcarbonates and alkoxides),[20–22] these aqueous SEIs were found to be predominantly inorganic metal fluorides (LiF or NaF),[13,15,16] originating from the reduction of salt anions bis(trifluoromethane sulfonyl)imide ($TFSI^-$) or trifluoromethane sulfonate (OTf^-). However, the formation of this anion-originated SEI faces a severe "cathodic challenge" as result of the repulsion of anions by negatively polarized anode surfaces,[5] making the expansion of cathodic limits extremely difficult. Further increasing the lithium salt concentration is apparently a non-sustainable approach even if the disadvantages such as cost and viscosity are not considered, because the cathodic limit only improves by ~0.10 V from a concentration increase from 21 m[13] to 28 m.[17] As such, most of the energy-dense anode materials still cannot be sufficiently supported by WiSE and its derivatives. Even lithiated titanate $Li_4Ti_5O_{12}$ (LTO), whose redox potential (1.55 V versus Li) sits near the cathodic limits of the water-in-bisalt electrolyte (21 m LiTFSI + 7 m LiOTf), fails to operate reversibly over the long term or to its full capacity, unless its surface is coated with an artificial interphase. The more expensive lithium salt based on bis(pentafluoroethane sulfonyl)imide (Beti) was reported to result in a slight expansion of the stability window at the anode side,[23] allowing LTO to operate on an Al current collector through kinetic suppression of hydrogen evolution. Additionally, an interphase artificially formed from fluorinated ether could even enable graphite or Li-metal cycling.[5] Such approaches still face questions of practicality in production, with either aggravated cost issue or limited cycling stability. Hence how to expand the cathodic limits of aqueous electrolytes in a cost-efficient way becomes a critical step in realizing practical high-voltage aqueous batteries.

In this work, we report a new class of electrolytes by hybridizing aqueous and non-aqueous solvents. Such electrolytes inherit the intrinsic merits of each system, and successfully resolve the conflicts among performance, cost, interphasial chemistry, sensitivity to ambient moisture, and environmental friendliness. Named hybrid aqueous/non-aqueous electrolyte (HANE), at an apparent LiTFSI concentration ~14 M, its aqueous portion brings non-flammability and non-toxicity characteristic of WiSE, while its non-aqueous portion (dimethyl carbonate [DMC]) introduces a secondary ingredient (alkylcarbonate) to the protective interphase on the anode in addition to the LiF from anion reduction. This hybrid interphase, consisting of LiF and alkylcarbonate, stabilizes the electrolyte down to 1.0 V versus Li, allowing LTO to deliver a reversible capacity of 160 mAh/g. The electrochemical stability window of HANE reaches 4.1 V, enabling a 3.2 V Li-ion cell chemistry constructed on LTO and $LiNi_{0.5}Mn_{1.5}O_4$ (LNMO), delivering a high energy density of 165 Wh/kg for >1,000 cycles. This hybridization approach provides an inspiration to reach a compromise between the completely different and often conflicting materials with the aim of maximizing the desired properties.

RESULTS

DMC has been the primary co-solvent used in LIBs, and its reduction results in the generation of lithium methyl carbonate (LMC) or Li_2CO_3. The latter is the subsequent reaction product of LMC with moisture/water, and it has been known as a Li^+ conductor with relatively low solubility in water. As a non-polar solvent (dielectric constant ε = 3.107, dipole moment 0.76), DMC is immiscible with the very polar water (dielectric constant ε = 80.10, dipole moment 1.85). However, the immiscibility

[1]Department of Chemical and Biomolecular Engineering, University of Maryland, College Park, College Park, MD 20742, USA

[2]Electrochemistry Branch, Sensor and Electron Devices Directorate, Power and Energy Division, U.S. Army Research Laboratory, Adelphi, MD 20783, USA

[3]Department of Physics & Astronomy, Hunter College of the City University of New York, New York, NY 10065, USA

[4]Lead Contact

*Correspondence: conrad.k.xu.civ@mail.mil (K.X.), cswang@umd.edu (C.W.)

https://doi.org/10.1016/j.joule.2018.02.011

Please cite this article in press as: Wang et al., Hybrid Aqueous/Non-aqueous Electrolyte for Safe and High-Energy Li-Ion Batteries, Joule (2018), https://doi.org/10.1016/j.joule.2018.02.011

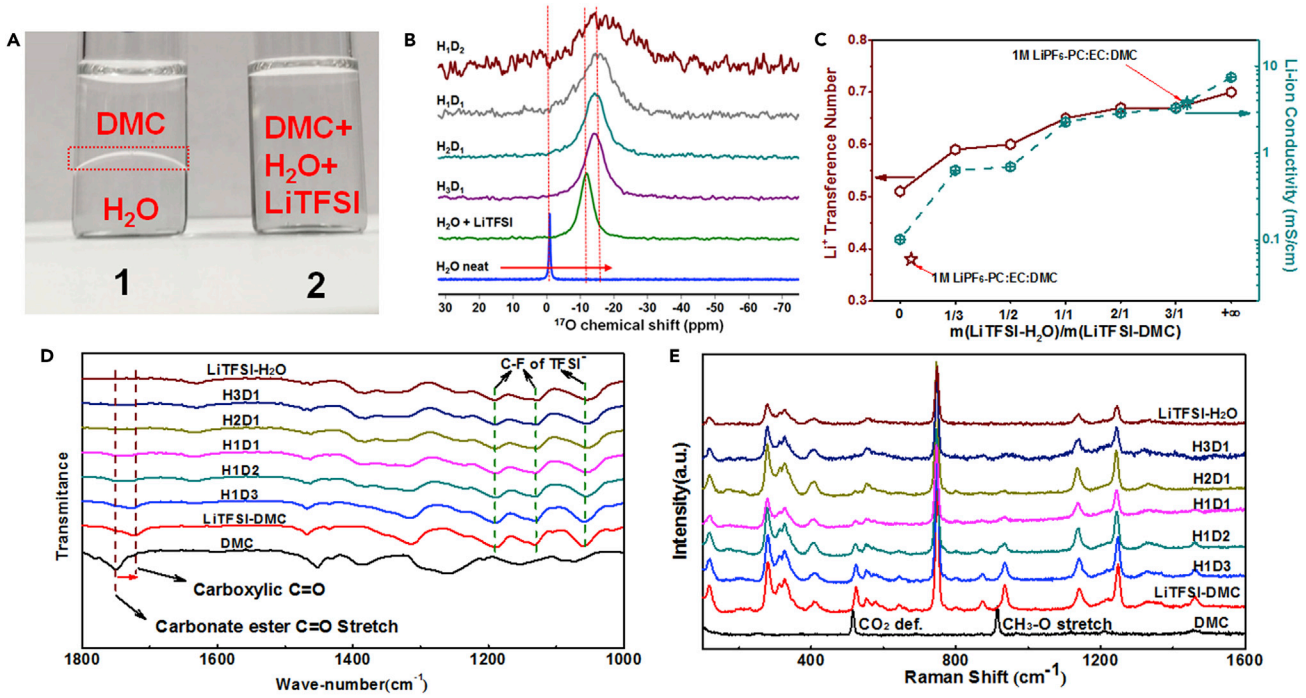

Figure 1. The Bulk Properties of Different Hybrid Electrolytes

(A) Immiscibility between H_2O and DMC, and the homogeneous HANE based on these two solvents.

(B) Chemical shifts for ^{17}O nuclei of H_2O in different aqueous and hybrid electrolytes.

(C) Li^+-transference number as derived from ^7Li- and ^{19}F-NMR spectra, and the Li^+−conductivities derived from the ion conductivities and Li^+-transference numbers. Also plotted as comparison are Li^+−conductivities for popular non-aqueous electrolyte 1.0 M $LiPF_6$ in PC/EC/DMC (data from Valøen and Reimers[24]).

(D and E) FTIR (D) and Raman spectra (E) of different electrolytes compared with pure aqueous (WiSE) and non-aqueous (9.25 m LiTFSI/DMC) electrolytes.

is altered by the presence of LiTFSI (Figure 1A). To prepare HANE at varying DMC/H_2O ratios, we first dissolved LiTFSI in DMC with a salt-to-solvent molar ratio of 1:1.2, then mixed this concentrated non-aqueous electrolyte (9.25 m LiTFSI) with WiSE (21 m LiTFSI) to yield a series of homogeneous solutions. For convenience, a HANE with LiTFSI-H_2O/LiTFSI-DMC mass ratios of x:y is denoted as H_xD_y hereafter. It is interesting to note that HANE of any H_xD_y ratio can be made without visible phase separation, indicating that LiTFSI strongly interacts with both aqueous and non-aqueous portions of the solution.

Various spectra were used to reveal the interplay among LiTFSI, DMC, and H_2O. Upon the introduction of non-aqueous solvent DMC, the chemical shift of ^{17}O nucleus in H_2O (δ = 0 ppm) experiences a steady decrease accompanied by peak broadening as observed by nuclear magnetic resonance (NMR, Figure 1B). Such a change reflects how the aqueous oxygen that is tightly coordinated with Li^+ becomes gradually deshielded as a competitive solvent intrudes into the Li^+-solvation sheath.[25] Multi-nuclei (^7Li and ^{19}F) NMR was used to measure the diffusivities of either Li^+ (D_{Li}) or $TFSI^-$ (D_F), from which Li^+-transference number (t_{Li}) was derived. It has been established that Li^+ in WiSE moves with unusually high transference numbers (t_{Li} > 0.73), because anions therein are relatively immobilized due to the uneven distribution of the limited population of H_2O molecules around Li^+ and the subsequent networked structure.[18] The Li^+ transference number for 9.25 M LiTFSI in DMC is ~0.45 (Figure 1C), which is higher than typical non-aqueous

Please cite this article in press as: Wang et al., Hybrid Aqueous/Non-aqueous Electrolyte for Safe and High-Energy Li-Ion Batteries, Joule (2018), https://doi.org/10.1016/j.joule.2018.02.011

electrolytes (t_{Li} ~ 0.3) due to the superconcentration. The introduction of the aqueous portion steadily raises the t_{Li}. In HANE H_1D_1 t_{Li} approaches 0.65, suggesting that the Li^+ transport in H_1D_1 is closer to aqueous electrolytes than to non-aqueous electrolytes. In other words, the average solvation structure around Li^+ should be dominated by aqueous solvent molecules (H_2O) rather than non-aqueous solvent molecules (DMC). Using t_{Li} and ion conductivities in Figure S1, Li^+ conductivities are also derived and plotted in comparison with a typical non-aqueous electrolyte, 1.0 M $LiPF_6$ in PC/EC/DMC.[24] Apparently, in the range between H_3D_1 and H_1D_3, the Li^+ conductivities are higher or at least comparable with the typical non-aqueous electrolytes (Figure 1C). In practical battery applications, such preferential Li^+ transport would favor the kinetics of cell chemistry, especially at high C rates. In these HANEs, ion conductivities are higher than the corresponding non-aqueous but lower than aqueous electrolytes (Figure S2).

On the other hand, in Fourier transformed infrared (FTIR) spectra (Figure 1D), the typical stretching mode of the carbonate ester carbonyl (C=O) in DMC (~1,750 cm^{-1}) shifted to lower wavenumber upon the addition of LiTFSI, which indicates its occupation by Li^+.[26–28] With increasing presence of aqueous portion, the C=O stretching mode weakens until its complete disappearance. A similar trend was observed in Raman spectra as well (Figure 1E), where the CO_2 deformation mode at ~520 cm^{-1} splits into multiple peaks upon addition of LiTFSI due to the breaking of the structural symmetry,[29–31] and, in the presence of aqueous portion, it decreases gradually in intensity. This change also applies to the CH_3-O stretching mode at ~935 cm^{-1}. The evolution of ^{17}O-NMR, FTIR, and Raman spectra all indicate that significant interaction exists among DMC, H_2O, and LiTFSI, leading to a new solvation structure that differs from those in the parental solutions of either aqueous or non-aqueous.

Molecular dynamics (MD) simulations were performed to shed light on the solvation structure in HANE H_1D_1 (Figures 2A and S3), revealing a pronounced ionic network with $TFSI^-$, H_2O, and DMC all participating in the Li^+ cation coordination. In this hybrid system, a Li^+ is often found bridging two $TFSI^-$ and has two solvents in its first coordination shell on average. A higher fraction of water than DMC in the Li^+ first coordination sheath is consistent with a 2.6 higher molar fraction of water than DMC in HANE (Figure S3). MD simulations further reveal the relationship between solution structure and electrochemical properties. The aggregate of $Li^+(TFSI)_2H_2O$ (indicated by the blue box in Figure 2A) is often observed in MD simulations. Such Li_2TFSI aggregates were previously shown to undergo reduction to form a LiF interphase below 2.9 V.[13,32] Importantly, many DMC molecules also coordinate Li^+, not only through the carbonyl oxygen (Oc) but also through the ethereal oxygen (EO), resulting in two Li^+ solvates bridged by DMC to form the Li^+_2(DMC), as highlighted by the red circle in Figure 2A. Analysis of MD simulation trajectories showed that around 20% of DMC molecules are coordinated by two Li^+ (Figure 2B). Such Li^+_2(DMC) solvates were also previously observed in the concentrated EC:DMC-$LiPF_6$ electrolytes in Born-Oppenheimer MD simulations and in the DMC-based crystal structures.[33]

The solvation environment of DMC greatly influences its reduction stability. The reduction potential for the Li^+(DMC) solvate is predicted from quantum chemistry calculations to be around of 0.35 V. It significantly increases to 1.38 V when two Li^+ coordinate DMC in the Li^+_2(DMC) solvate shown in Figure 2C due to additional stabilization of the excess electron on the DMC molecule by two Li^+(Figure S4). Thus, highly concentrated electrolytes with a high fraction of Li^+_2(DMC) solvates have a significantly higher onset

Please cite this article in press as: Wang et al., Hybrid Aqueous/Non-aqueous Electrolyte for Safe and High-Energy Li-Ion Batteries, Joule (2018), https://doi.org/10.1016/j.joule.2018.02.011

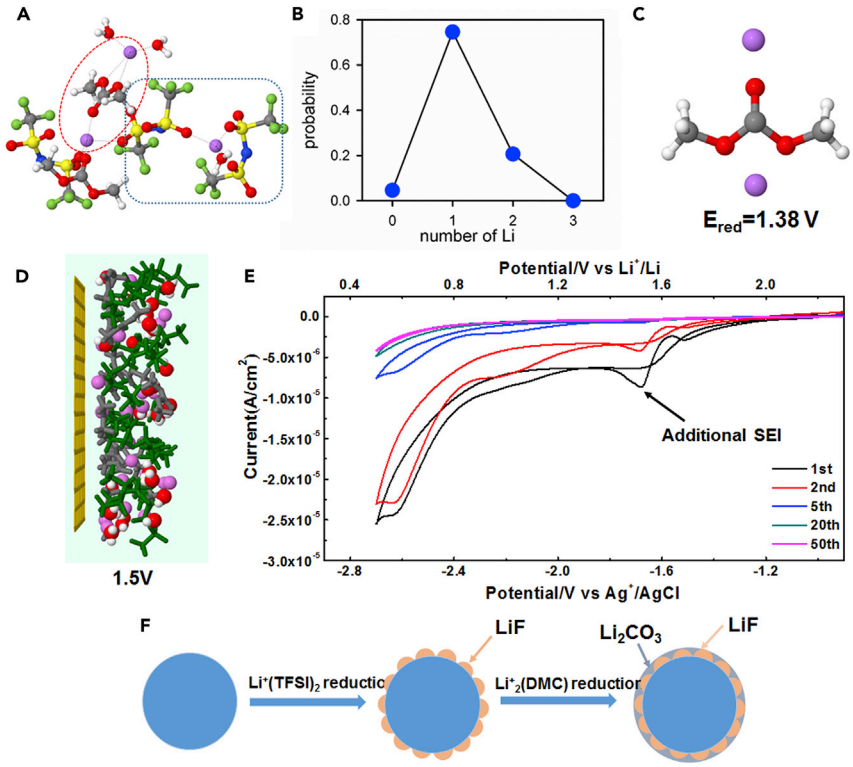

Figure 2. The MD Simulations and the Cathodic Interphasial Properties of the HANE H_1D_1

(A) Representative liquid structure for the H_1D_1HANE. Colors: Li^+, purple; O, red; C, gray; H, white; N, blue; S, yellow; F, green.

(B) Predicted reduction potentials from G4MP2 quantum chemistry calculation.

(C) The probability of DMC$(Li^+)_n$ solvates with nLi^+ cation within 4.5 Å of the carbonyl carbon of DMC.

(D) Snapshots of the interfacial regions at 1.5 V (gray, DMC; purple, lithium; green, $TFSI^-$) from MD simulations of the graphite|H_1D_1HANE interfaces.

(E) Cyclic voltammetry (CV) of the aluminum electrode in H_1D_1HANE using a three-electrode cell with activated carbon and Ag/AgCl as counter and reference electrodes, respectively, at a scan rate of 5 mV/s. The potential has been converted to Li reference for convenience.

(F) Schematic illustration of the anode SEI formation in HANE.

of electrolyte reduction compared with dilute DMC-based electrolytes. Reduction of Li^+DMC is known to lead to formation of Li semi-carbonates or Li_2CO_3 that have low solubility in water and would precipitate, forming an SEI.[27,34,35]

The presence of the Li_2DMC and Li_2TFSI aggregates in bulk and interfacial electrolyte layers on the anode (see Figures 2D and S5) indicates that both TFSI and DMC likely participate in the interphasial chemistry, and support for the hypothesis about the stepwise formation of the SEI was evidenced by the electrochemical behavior shown in the cyclic voltammetry (Figure 2E). During the initial scan, a reduction peak at ~1.5 V versus Li was presented and disappeared after the fifth scan, consistent with the reduction of Li_2DMC solvates predicted by modeling. This typical passivation phenomenon should be ascribed to the formation process of an interphase, which results in the further extension of the cathodic limit to ~1.0 V versus Li, much lower than what WiSE could achieve (Figure S6). It is reasonable to conclude that H_2O reduction was further suppressed owing to the formation of an additional interphase driven by the reduction of DMC. An interphase consisting of distinct chemical species from $TFSI^-$ and DMC solvent was thus hinted at from the solvation sheath structure and the

Please cite this article in press as: Wang et al., Hybrid Aqueous/Non-aqueous Electrolyte for Safe and High-Energy Li-Ion Batteries, Joule (2018), https://doi.org/10.1016/j.joule.2018.02.011

electrochemical behavior, with both LiF and Li_2CO_3 as the main components of construction of the SEI (Figure 2F). As the direct consequence of the unique Li^+-solvation structure in HANE, the unusual interphasial structure constructed by this stepwise formation mechanism could lead to an interphase that more effectively blocks the electron tunnel while better conducting Li^+ across it.

The anodic limits for HANE are closely related to how H_2O, DMC molecules, and anions adsorb at the inner-Helmholtz interface of the electrode as a function of electrode potential,[5] as revealed by the MD simulations (Figure S5). H_2O tends to desorb from the electrode proximity as the electrode is positively polarized, accompanied by the simultaneous increase in H_2O population in a second layer. $TFSI^-$ and DMC are strongly adsorbed on the electrode surface, which shields H_2O molecules from direct interaction with the cathode surface and minimizes oxygen evolution at the high potential of 4.5 V (Figure 3A), as expected from the higher nucleophilicity of both $TFSI^-$ and DMC. Such preferential adsorption leads to a higher anodic limit of HANE, as it has been also responsible for the high anodic stability of WiSE and is in agreement with the previous observations for other concentrated electrolytes.[36] An anodic limit of ~5.1 V versus Li was conservatively demonstrated from the cyclic voltammetry conducted on Pt electrodes (Figure 3B), and the oxygen evolution current decreased significantly compared with WiSE (Figure S7). Combined with the extended cathodic limit due to the interphase on the anode, an overall electrochemical stability window of 4.1 V is now available, providing desired flexibility in selecting electrode materials that are otherwise forbidden in the dilute or even concentrated WiSE aqueous electrolytes.

The expanded electrochemical stability window for H_1D_1HANE was further verified by active electrode materials based on spinel LTO and LNMO. Though safely enveloped by the electrochemical stability window of non-aqueous electrolytes, the application of LTO in aqueous electrolytes has always been problematic because of the "cathodic challenge"[5,14] (Figure S8) and titanate's natural tendency in catalytically splitting water. Even with the so-called hydrate melt based on LiTFSI and LiBeti (equivalence of ~28 m concentrated aqueous solution), LTO is only partially stabilized, while its full capacity can only be accessible at very high C rates on Al current collectors to circumvent the effect of hydrogen evolution.[23] However, as the additional interphase layers formed in HANE along with water activity further suppressed therein because of the presence of DMC, the reversible lithiation-delithiation of LTO became possible (Figure 3B), even at low C rates. On the other hand, the high anodic stability of 5.1 V well accommodates the redox reaction of the LNMO cathode (4.96 V/4.82 V). Hence, a 3.2 V aqueous cell constructed on LTO-LNMO (mass ratio 1:2) was assembled and evaluated in HANE. A low current density of 0.5 C instead of a high rate was used to demonstrate the authentic stability of HANE at the extreme electrode potentials. Such an LTO-LNMO full cell delivers a voltage plateau at 3.0–3.2 V during both charging and discharging processes. The discharging capacity based on the LTO mass is 163 mAh/g, near its theoretical capacity (175 mAh/g),[37,38] confirming the full utilization of LTO in HANE. In the first cycle, a coulombic efficiency of 83.5% indicates the relative amount of HANE consumed to form the SEI on the anode along with some H_2O decomposition, while in the second cycle the voltage profile of the discharge already becomes nearly identical to the first discharge, suggesting the near completion of interphase formation. The energy density of this aqueous full cell achieves 165 Wh/kg (55 Ah/kg and 3.0 V average discharge potential) based on the first discharge curve (Figure S9), which is comparable with those of the non-aqueous Li-ion cells (160 Wh/kg for $LiMn_2O_4/Li_4Ti_5O_{12}$[39] or 168 Wh/kg for $LiFePO_4/Li_4Ti_5O_{12}$[40,41]). Further optimization

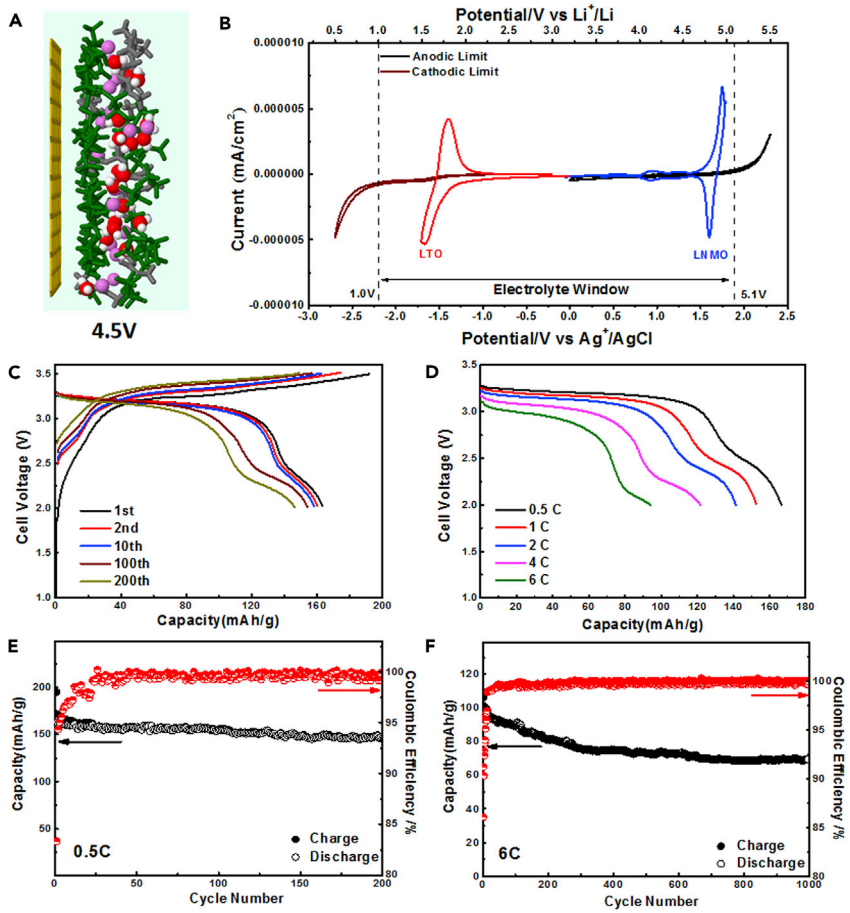

Figure 3. The Anodic Interphasial Structure and the lectrochemical Performance of the LTO-LNMO Full Cell

(A) Snapshots of the interfacial regions at the cathode surface (gray, DMC; purple, lithium; green, $TFSI^-$) from MD simulations of the graphite|H_1D_1HANE interfaces.

(B) Electrochemical stability window of the H_1D_1HANE measured with CV on current collectors as well as active electrodes (LTO and LNMO). The cathodic and anodic limits were separately tested using Al and Pt working electrodes, respectively, with activated carbon and Ag/AgCl as counter and reference electrodes, respectively, at a scan rate of 5 mV/s, wherein the cathodic limit was the 20th cycle shown in Figure 2E. The CV of active electrodes (LTO and LNMO) was tested at 0.5 mV/s.

(C) Typical voltage profiles of LTO-LNMO full cell at a constant current of 0.5 C (both capacity and rate are based on LTO mass).

(D) The discharge voltage profiles of the LTO-LNMO cell at various rates.

(E and F) Cycling stability and coulombic efficiency of LTO-LNMO full cell at constant currents of 0.5 C (E) and 6 C (F).

in the cell design and engineering may improve the initial coulombic efficiency and bring the full cell energy density closer to the theoretical value of 255 Wh/kg. The rate capability of the LTO-LNMO cell in HANE was also evaluated (Figure 3D). The cell maintains a discharge capacity of 94 mAh/g at 6 C, which corresponds to 58% of its capacity at 0.5 C. The interphasial chemistry from both aqueous and non-aqueous components must have stabilized the LTO surface substantially, because the coulombic efficiency of the full cell increased from 94.3% of the second cycle to nearly 100% after only 20 cycles (Figure 3E). Excellent cycling stability ensued, with capacity decay rates per cycle of 0.053% and 0.024% at 0.5 C for 200 cycles (Figure 3E) and at 6 C for 1,000 cycles (Figure 3F), respectively.

Please cite this article in press as: Wang et al., Hybrid Aqueous/Non-aqueous Electrolyte for Safe and High-Energy Li-Ion Batteries, Joule (2018), https://doi.org/10.1016/j.joule.2018.02.011

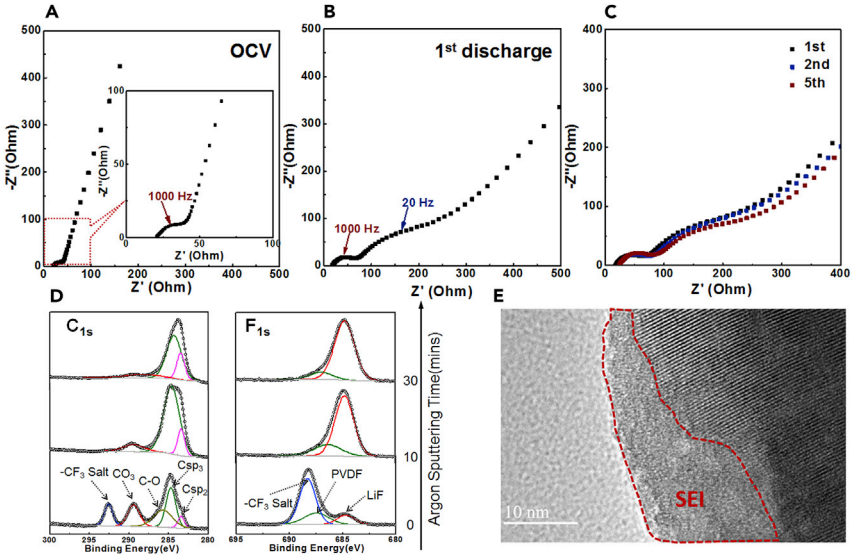

Figure 4. EIS Spectroscopy and the SEI Characterization of the LTO Surface

(A–C) Electrochemical impedance spectroscopy of the LTO-LNMO cell at the open circuit voltage state (A), after the first charge-discharge state (B), and after different cycles (C).

(D and E) X-ray photoelectron spectroscopy (XPS) (D) and transmission electron microscopy (E) image of fully lithiated LTO electrodes. The cells were charged at 3.5 V before LTO was recovered, and the depth-profile in XPS was established via various durations of Ar^+ sputtering. SEI, solid-electrolyte interphase.

DISCUSSION

The interphase between electrode and HANE was further analyzed using the electrochemical impedance spectrum (EIS),[42–44] which was conducted on the LTO/LMNO full cell before and after the first charge-discharge cycle (Figures 4A and 4B), respectively. An additional semicircle at the frequency of ~20 Hz observed in Figure 4B was attributed to the newly formed interphase.[45] After the first cycle, the impedance spectra became constant in all subsequent cycles (Figure 4C), indicating the near completion of the interphasial formation process in the first cycle. This high efficiency of interphase formation, as well as the outstanding protection effectiveness of such interphases in insulating sustained electrolyte decomposition, has been witnessed by voltage profiles in Figure 3C. X-ray photoelectron spectroscopy (XPS) was conducted on the lithiated LTO anode that was recovered after charging to 3.5 V in the first charging process. The binding energies for the 1s valence electrons of C and F are shown in Figure 4D. The F1s signal can be deconvoluted into contributions from the binder polyvinylidene fluoride (670 eV) used in the composite electrode, certain CF_3 species apparently generated by the salt anion $TFSI^-$ (687.5 eV), and inorganic fluoride LiF (684.5 eV), among which LiF is the most insignificant. However, when the top layer of the interphase is gradually removed under Ar^+ sputtering, LiF becomes the dominant species, indicating that the interphase formation could have started with the early reduction of $TFSI^-$. Meanwhile, the C1s signals can also be deconvoluted into CF_3 species (293 eV), carbonyl (C=O) of alkylcarbonates (289 eV), ethereal (C-O) species (286 eV), and various sp3 or sp2 elemental carbon species below 284 eV. While the latter should be attributed to the conductive carbon used in the composite electrode, the CF_3 species apparently comes from $TFSI^-$ or its fragments as result of the incomplete reduction process. The organic species (carbonyl and ethereal) arise from the reduction of the Li^+_2(DMC) solvation aggregates, which have been frequently observed in

Please cite this article in press as: Wang et al., Hybrid Aqueous/Non-aqueous Electrolyte for Safe and High-Energy Li-Ion Batteries, Joule (2018), https://doi.org/10.1016/j.joule.2018.02.011

interphases formed in non-aqueous electrolytes. By contrast, only a very small peak of alkylcarbonates or Li_2CO_3 was detected on the anode recovered after charging to 2.7 V, with LiF still present in high abundance (Figure S10), consistent with the different reduction potentials of LiTFSI(H_2O) clusters in WiSE (2.90 V versus Li) and Li^+_2(DMC) solvation aggregates (1.38 V versus Li) as predicted by MD simulations. The thickness of such interphases is revealed by transmission electron microscopy (TEM) to be in the range of ~10 nm (Figure 4E), which completely covers the surface of LTO. Since LiF is a poor Li^+ conductor, it has always puzzled us how a LiF-dominated SEI functions, given the excellent rate capabilities observed experimentally. In the interphases formed in the current HANE, the additional interphasial component alkylcarbonate resulting from the DMC reduction at lower electrode potentials could serve as an assisting phase, whose boundary with LiF crystallites would create a much more conductive pathway according to the space-charge model proposed by Qi and co-workers.[46] On the other hand, no obvious interphase layer was observed from the TEM image of the cycled LNMO (Figure S11), in excellent agreement with previous observations made on LMO ($LiMn_2O_4$) cycled in WiSE,[13] as well as the MD simulations made on the structure near the inner-Helmholtz layers.[5]

Finally, various safety tests on materials were performed to confirm that the intrinsically safe nature brought by the aqueous component, WiSE, was not compromised by the introduction of a non-aqueous component. Differential scanning calorimetry (DSC) demonstrates that the basic thermal behavior of H_1D_1 HANE is essentially identical to that of WiSE (Figure S12) with no significant exothermic peak observed before 300°C. In the presence of a charged anode (lithiated LTO) and cathode (delithiated LMNO), no major reactions can be detected for H_1D_1 HANE until the DSC hermetical pan burst at 210°C and 225°C, respectively (Figure S13A). In sharp contrast, the non-aqueous electrolytes react violently with these electrodes, as evidenced by the significant exothermic peaks at about 115°C (Figure S13B). More visual results were demonstrated in the open flame combustion test (Figure S14) using a propane-oxygen torch (~2,600°C). Besides solvent boiling and evaporation, no HANE combustion was observed despite the DMC present. Hence, we can conclude with confidence that HANE maintains the same safety level as its WiSE ancestor, and would make the Li-ion cells based on such hybrid electrolytes safe.

In summary, we developed a brand-new class of hybrid electrolyte that bridges the gap between aqueous and non-aqueous electrolytes. Such electrolytes inherit the merits of both parent systems and enable a 3.2 V class aqueous Li-ion chemistry with high energy density, cycling stability, and intrinsic safety. The introduction of the non-aqueous component pushes the cathodic limit of the hybrid electrolyte down to ~1.0 V with the formation of a hierarchical interphase, and extends the anodic limit to 5.1 V. The Li-ion full cell constructed with LTO and high-voltage LMNO in HANE delivered a high working voltage of 3.2 V and a high energy density of 165 Wh/kg for >1,000 cycles, comparable with some state-of-the-art LIBs using non-aqueous electrolytes. More importantly, the overall LiTFSI concentration was reduced by 15.4% per unit volume of H_1D_1 HANE as compared with WiSE (Table S1), easing the cost concern imposed by LiTFSI. The aqueous component of the system, WiSE, ensures its safety against both electrochemical reactions and combustion. The unique hybridization approach described in this work not only provides a brand-new and practical electrolyte system for aqueous battery chemistries, but also serves as an inspiration for finding a compromise for the conflicting properties of different materials while maximizing their benefits.

EXPERIMENTAL PROCEDURES

Full details of all experiments are provided in Supplemental Experimental Procedures.

SUPPLEMENTAL INFORMATION

Supplemental Information includes Supplemental Experimental Procedures, 14 figures, and 1 table and can be found with this article online at https://doi.org/10.1016/j.joule.2018.02.011.

ACKNOWLEDGMENTS

The principal investigators (K.X. and C.W.) gratefully acknowledge the funding support from DOE ARPA-E (DEAR0000389) and Center of Research on Extreme Batteries (CREB). We also acknowledge the support of the Maryland Nano Center and its NispLab. The NispLab is supported in part by the NSF as an MRSEC Shared Experimental Facility. F.W. and J.V. were supported by the Oak Ridge Associated Universities (ORAU) through contracts W911NF-16-2-0202 and W911NF-16-2-0107.

AUTHOR CONTRIBUTIONS

F.W., K.X., and C.W. conceived the idea and co-wrote the manuscript. F.W., W.S., and N.E. carried out the synthesis, material characterizations, and electrochemical evaluation. J.V. and O.B. conducted MD simulations and QC calculations. X.F., T.G., M.S.D., M.G., Y.L., and S.G. assisted with the material characterizations.

DECLARATION OF INTERESTS

The authors declare no competing interests.

Received: January 2, 2018
Revised: February 1, 2018
Accepted: February 12, 2018
Published: March 12, 2018

REFERENCES

1. Armand, M., and Tarascon, J.M. (2008). Building better batteries. Nature *451*, 652–657.

2. Dunn, B., Kamath, H., and Tarascon, J.M. (2011). Electrical energy storage for the grid: a battery of choices. Science *334*, 928–935.

3. Li, Y., Zhou, W., Xin, S., Li, S., Zhu, J., Lü, X., Cui, Z., Jia, Q., Zhou, J., and Zhao, Y. (2016). Fluorine-doped antiperovskite electrolyte for all-solid-state lithium-ion batteries. Angew. Chem. Int. Ed. *55*, 9965–9968.

4. Liu, Y., Fang, S., Luo, D., Yang, L., and Hirano, S.I. (2016). Safe electrolytes for lithium-ion batteries based on ternary mixtures of triethylene glycol dimethylether, fluoroethylene carbonate and non-flammable methyl-nonafluorobutyl ether. J. Electrochem. Soc. *163*, A1951–A1958.

5. Yang, C., Chen, J., Qing, T., Fan, X., Sun, W., von Cresce, A., Ding, M.S., Borodin, O., Vatamanu, J., and Schroeder, M.A. (2017). 4.0 V aqueous Li-ion batteries. Joule *1*, 122–132.

6. Parker, J.F., Chervin, C.N., Pala, I.R., Machler, M., Burz, M.F., Long, J.W., and Rolison, D.R. (2017). Rechargeable nickel-3D zinc batteries: an energy-dense, safer alternative to lithium-ion. Science *356*, 415–418.

7. Wang, F., Lin, Y., Suo, L., Fan, X., Gao, T., Yang, C., Han, F., Qi, Y., Xu, K., and Wang, C. (2016). Stabilizing high voltage $LiCoO_2$ cathode in aqueous electrolyte with interphase-forming additive. Energy Environ. Sci. *9*, 3666–3673.

8. Li, W., Dahn, J.R., and Wainwright, D.S. (1994). Rechargeable lithium batteries with aqueous-electrolytes. Science *264*, 1115–1118.

9. Luo, J.Y., Cui, W.J., He, P., and Xia, Y.Y. (2010). Raising the cycling stability of aqueous lithium-ion batteries by eliminating oxygen in the electrolyte. Nat. Chem. *2*, 760–765.

10. Wang, Y., Yi, J., and Xia, Y. (2012). Recent progress in aqueous lithium-ion batteries. Adv. Energy Mater. *2*, 830–840.

11. Kim, H., Hong, J., Park, K.Y., Kim, H., Kim, S.W., and Kang, K. (2014). Aqueous rechargeable Li and Na ion batteries. Chem. Rev. *114*, 11788–11827.

12. Ramanujapuram, A., Gordon, D., Magasinski, A., Ward, B., Nitta, N., Huang, C., and Yushin, G. (2016). Degradation and stabilization of lithium cobalt oxide in aqueous electrolytes. Energy Environ. Sci. *9*, 1841–1848.

13. Suo, L., Borodin, O., Gao, T., Olguin, M., Ho, J., Fan, X., Luo, C., Wang, C., and Xu, K. (2015). "Water-in-salt" electrolyte enables high-voltage aqueous lithium-ion chemistries. Science *350*, 938–943.

14. Wang, F., Suo, L., Liang, Y., Yang, C., Han, F., Gao, T., Sun, W., and Wang, C. (2017). Spinel $LiNi_{0.5}Mn_{1.5}O_4$ cathode for high-energy aqueous lithium-ion batteries. Adv. Energy Mater. *7*, https://doi.org/10.1002/aenm.201600922.

15. Suo, L., Oh, D., lin, y., Zhuo, Z., Borodin, O., Gao, T., wang, f., Kushima, A., Wang, Z., Kim, H.C., et al. (2017). How solid-electrolyte-interphase forms in aqueous electrolytes. J. Am. Chem. Soc. *139*, 18670–18680.

16. Suo, L., Borodin, O., Wang, Y., Rong, X., Sun, W., Fan, X., Xu, S., Schroeder, M.A., Cresce, A.V., and Wang, F. (2017). "Water-in-salt" electrolyte makes aqueous sodium-ion battery safe, green, and long-lasting. Adv. Energy Mater. *7*, https://doi.org/10.1002/aenm.201701189.

17. Suo, L., Borodin, O., Sun, W., Fan, X., Yang, C., Wang, F., Gao, T., Ma, Z., Schroeder, M., and von Cresce, A. (2016). Advanced high-voltage aqueous lithium-ion battery enabled by "water-in-bisalt" electrolyte. Angew. Chem. Int. Ed. *55*, 7136–7141.

18. Borodin, O., Suo, L., Gobet, M., Ren, X., Wang, F., Faraone, A., Peng, J., Olguin, M., Schroeder, M., and Ding, M.S. (2017). Liquid structure with nano-heterogeneity promotes cationic transport in concentrated electrolytes. ACS Nano *11*, 10462–10471.

19. Yang, C., Suo, L., Borodin, O., Wang, F., Sun, W., Gao, T., Fan, X., Hou, S., Ma, Z., Amine, K., et al. (2017). Unique aqueous Li-ion/sulfur chemistry with high energy density and reversibility. Proc. Natl. Acad. Sci. USA *114*, 6197–6202.

20. Xu, K. (2014). Electrolytes and interphases in Li-ion batteries and beyond. Chem. Rev. *114*, 11503–11618.

21. Gauthier, M., Carney, T.J., Grimaud, A., Giordano, L., Pour, N., Chang, H.H., Fenning, D.P., Lux, S.F., Paschos, O., Bauer, C., et al. (2015). Electrode-electrolyte interface in Li-ion batteries: current understanding and new insights. J. Phys. Chem. Lett. *6*, 4653–4672.

22. Delp, S.A., Borodin, O., Olguin, M., Eisner, C.G., Allen, J.L., and Jow, T.R. (2016). Importance of reduction and oxidation stability of high voltage electrolytes and additives. Electrochim. Acta *209*, 498–510.

23. Yamada, Y., Usui, K., Sodeyama, K., Ko, S., Tateyama, Y., and Yamada, A. (2016). Hydrate-melt electrolytes for high-energy-density aqueous batteries. Nat. Energy *1*, 16129.

24. Valøen, L.O., and Reimers, J.N. (2005). Transport properties of $LiPF_6$-based Li-ion battery electrolytes. J. Electrochem. Soc. *152*, A882–A891.

25. Ding, M.S., von Cresce, A., and Xu, K. (2017). Conductivity, viscosity, and their correlation of a super-concentrated aqueous electrolyte. J. Phys. Chem. C *121*, 2149–2153.

26. Chapman, N., Borodin, O., Yoon, T., Nguyen, C.C., and Lucht, B.L. (2017). Spectroscopic and density functional theory characterization of common lithium salt solvates in carbonate electrolytes for lithium batteries. J. Phys. Chem. C *121*, 2135–2148.

27. Seo, D.M., Reininger, S., Kutcher, M., Redmond, K., Euler, W.B., and Lucht, B.L. (2015). Role of mixed solvation and ion pairing in the solution structure of lithium ion battery electrolytes. J. Phys. Chem. C *119*, 14038–14046.

28. Cresce, A.V., Russell, S.M., Borodin, O., Allen, J.A., Schroeder, M.A., Dai, M., Peng, J., Gobet, M.P., Greenbaum, S.G., and Rogers, R.E. (2017). Solvation behavior of carbonate-based electrolytes in sodium ion batteries. Phys. Chem. Chem. Phys. *19*, 574–586.

29. Katon, J., and Cohen, M. (1975). The vibrational spectra and structure of dimethyl carbonate and its conformational behavior. Can. J. Chem. *53*, 1378–1386.

30. Morita, M., Asai, Y., Yoshimoto, N., and Ishikawa, M. (1998). A Raman spectroscopic study of organic electrolyte solutions based on binary solvent systems of ethylene carbonate with low viscosity solvents which dissolve different lithium salts. J. Chem. Soc. Faraday Trans. *94*, 3451–3456.

31. Bohets, H., and van der Veken, B.J. (1999). On the conformational behavior of dimethyl carbonate. Phys. Chem. Chem. Phys. *1*, 1817–1826.

32. Yamada, Y., and Yamada, A. (2017). Superconcentrated electrolytes to create new interfacial chemistry in non-aqueous and aqueous rechargeable batteries. Chem. Lett. *46*, 1056–1064.

33. Borodin, O., Olguin, M., Ganesh, P., Kent, P.R.C., Allen, J.L., and Henderson, W.A. (2016). Competitive lithium solvation of linear and cyclic carbonates from quantum chemistry. Phys. Chem. Chem. Phys. *18*, 164–175.

34. Yoon, T., Milien, M.S., Parimalam, B.S., and Lucht, B.L. (2017). Thermal decomposition of the solid electrolyte interphase (SEI) on silicon electrodes for lithium ion batteries. Chem. Mater. *29*, 3237–3245.

35. Seo, D.M., Chalasani, D., Parimalam, B.S., Kadam, R., Nie, M., and Lucht, B.L. (2014). Reduction reactions of carbonate solvents for lithium ion batteries. ECS Electrochem. Lett. *3*, A91–A93.

36. Vatamanu, J., and Borodin, O. (2017). Ramifications of water-in-salt interfacial structure at charged electrodes for electrolyte electrochemical stability. J. Phys. Chem. Lett. *8*, 4362–4367.

37. Ge, H., Li, N., Li, D., Dai, C., and Wang, D. (2009). Study on the theoretical capacity of spinel lithium titanate induced by low-potential intercalation. J. Phys. Chem. C *113*, 6324–6326.

38. Jung, H.G., Jang, M.W., Hassoun, J., Sun, Y.K., and Scrosati, B. (2011). A high-rate long-life $Li_4Ti_5O_{12}$/Li $[Ni_{0.45}Co_{0.1}Mn_{1.45}]$ O_4 lithium-ion battery. Nat. Commun. *2*, 516.

39. Börner, M., Klamor, S., Hoffmann, B., Schroeder, M., Nowak, S., Würsig, A., Winter, M., and Schappacher, F. (2016). Investigations on the C-rate and temperature dependence of manganese dissolution/deposition in $LiMn_2O_4$/$Li_4Ti_5O_{12}$ lithium ion batteries. J. Electrochem. Soc. *163*, A831–A837.

40. Julien, C.M., Zaghib, K., Mauger, A., and Groult, H. (2012). Enhanced electrochemical properties of $LiFePO_4$ as positive electrode of Li-ion batteries for HEV application. Adv. Chem. Eng. Sci. *2*, 321.

41. Chu, S., Cui, Y., and Liu, N. (2017). The path towards sustainable energy. Nat. Mater. *16*, 16–22.

42. Zhang, S.S., Xu, K., and Jow, T.R. (2006). EIS study on the formation of solid electrolyte interface in Li-ion battery. Electrochim. Acta *51*, 1636–1640.

43. Qin, Y., Chen, Z., Liu, J., and Amine, K. (2010). Lithium tetrafluoro oxalato phosphate as electrolyte additive for lithium-ion cells. Electrochem. Solid State Lett. *13*, A11.

44. Pfanzelt, M., Kubiak, P., Jacke, S., Dimesso, L., Jaegermann, W., and Wohlfahrt-Mehrens, M. (2012). SEI formation on TiO_2 rutile. J. Electrochem. Soc. *159*, A809.

45. Steinhauer, M., Risse, S., Wagner, N., and Friedrich, K.A. (2017). Investigation of the solid electrolyte interphase formation at graphite anodes in lithium-ion batteries with electrochemical impedance spectroscopy. Electrochim. Acta *228*, 652–658.

46. Zhang, Q., Pan, J., Lu, P., Liu, Z., Verbrugge, M.W., Sheldon, B.W., Cheng, Y.T., Qi, Y., and Xiao, X. (2016). Synergetic effects of inorganic components in solid electrolyte interphase on high cycle efficiency of lithium ion batteries. Nano Lett. *16*, 2011–2016.